



Optimum Diameter and Location of Pipes Containing Phase Change Materials in a Channel in Latent and Sensible Heat Transfer

J. Rostami*

Department of Mechanical Engineering, Razi University, Kermanshah, Iran

ABSTRACT: In this paper, two pipes containing phase change materials, located perpendicular to the flow direction in a channel, are simulated numerically to find out their best diameter and location (their distances from the walls) in the convective heat transfer behavior. The governing equations have been solved by the semi-implicit method for pressure linked equations. In the first part, the phase change material is in the phase change (isothermal state) process, and the best location and diameter of the pipes are defined. In the second part, for obtained best size and location obtained in the first part, depending on the phase change material to the fluid special heat capacity ratio, the duration of the after-melting process, and reaching the final equilibrium state of the phase change material has been determined. The results of the first part show the best geometrical parameter depends on the Reynolds and the Prandtl numbers. Results of the second part show, the time at which the temperature of the pipes (phase change material) reaches 99% of the temperature of the inlet flow, depends on the special heat capacity ratio. Also, the best non-dimensional diameter of pipes is 0.153 for $Re=500$ and 0.165 for $Re=700$ in different Prandtl numbers and the best non-dimensional distance of the pipes from the wall is between 0.15-0.175 for different Reynolds and Prandtl numbers.

Review History:

Received: May, 04, 2020

Revised: Feb. 09, 2021

Accepted: Aug. 28, 2021

Available Online: Mar. 04, 2021

Keywords:

Body fitted mesh

Non-orthogonal grid

Phase change material

Sensible heat transfer

Latent heat transfer

1- Introduction

Phase Change Materials (PCMs) have special properties and behavior in heat transfer processes. These materials in phase change duration (such as a mixture of ice and water) get the heat as a latent heat without temperature increasing. On the other hand, they appear as heat sinks and increase the heat transfer rate. They are used in air conditioning to reduce the power consumption of the chiller by making ice in the times with low electricity load of the city and just by turning on the fan of the system with low energy consumption bypass the ambient air on the PCM containers to supply cool air for rooms. Another application of this study is using micro-pipes contains PCM to cool the mini-electronic devices. Then the PCMs are favorable materials for researchers and have been studied by many authors.

Hu et al. [1] studied a PCM solar air heat exchanger and its ventilation preheating effectiveness numerically and experimentally. The system in their study has been designed to improve the air quality with solar energy. The flow is laminar and the buoyancy force is used in the governing equations. Finally, the optimum state of using PCM has been obtained for their solar system. Khan et al. [2] investigated the building wall heat transfer using PCM. The effect of PCM on the heat transfer rate by two models of the building wall fragments was studied experimentally. In the first model, the location

of the PCM in the wall was changed to find out the optimum state in heat transfer. In the second model, the PCM effects in presence of air gap in the wall have been studied. Arici et al. [3] studied PCM integrated to external building walls to find out an optimum situation including location, thickness and melting temperature of the PCM in different climates in three cities of Turkey has been explored. They showed that the optimized melting temperature and PCM layer thickness vary from 6 to 34°C and 1 to 20 mm depending on climatic conditions. Desai et al. [4] investigated the fin efficiency for PCM based thermal control module numerically. The weakness of the PCMs is their low thermal conductivity. One way to improve the efficiency of the PCM is using conducting fins in it. They studied different numbers and shapes of the fins and found that 100 triangular fins are the best configuration. Chen et al. [5] investigated the latent heat thermal storage unit with PCM in the inner side of a tube experimentally and numerically. They compared the system performance when the inside of the tube is filled by PCM with different rates (40 to 90%). The results show that for the filling rate of 62% a better performance will be achieved in comparison with the state that the outer part is filled with PCM. The effect of the presence of the rectangular fins in a PCM has been investigated by Mazhar et al. [6]. The optimum configuration of fins for heat transfer enhancement is using rectangular 40×90 mm copper plates with 10 mm pitch. Heat transfer of thermal energy storage for PCM melting in the horizontal tube has

*Corresponding author's email: jrostami@razi.ac.ir



been investigated by Aadmi et al. [7] numerically and experimentally. Thermal conductivity, heat capacity, and ability to store and release the thermal energy of PCM which is made of Epoxy resin, copper tube, and paraffin wax have been measured and validated by numerical results. The effects of the radius of the cylinder on the melting time of the PCM have been studied. Aziz et al. [8] simulated heat transfer enhancement in a thermal energy storage tank containing a spherical encapsulated PCM. Three models of the spherical PCMs which are made of plain plastic, plain plastic with conducting pins, and plain plastic covered by copper and equipped with pins were studied. Their results show that the phase change time in the second case reduces by 27% and in the third case, it reduces by 37%. Cabeza et al. [9] investigated the heat transfer in water as a PCM in thermal energy storage. They used three methods to enhance the heat transfer in cold storage working with water-ice as PCM. The first one was adding pieces of stainless steel, the second one was adding copper pieces and the third one was adding graphite. They concluded that graphite has more effect on the heat transfer rate than the other ones. Chen et al. [10] studied heat transfer of PCMs used in a box-type solar cooker, numerically. Two-dimensional enthalpy approach simulation was used and the melt fraction by conduction has been calculated. They showed that for a PCM with low thermal conductivity the material of the heat exchanger container has a sensitive effect on melt fraction. Also, the initial temperature of the PCM is not so important. But, the wall temperature has a significant effect on the melting fraction. Chow and Lyu [11] analyzed the advantage of PCM heat exchanger in liquid flow window numerically. This window can save considerable energy in buildings by supplying the needed warm water. Their results show that using PCM, supply 31.4% and 11.4% more hot water in summer and winter for buildings, respectively. Khan et al. [12] evaluated the metal oxides based nano-PCMs for latent heat storage. The base PCM is paraffin and the problem consists of natural convection in shell and tube heat exchangers. They showed that an increase in the volume concentration of the nanoparticles reduces the natural convection effects. Inclined heat sink with finned PCM container for solar application has been analyzed thermally by Sathe and Dhoble [13]. Unsteady numerical natural convection using Boussinesq approximations with change in PCM thicknesses (20 to 30 mm), inclination angles (30 to 90°) and the number of extended surfaces (2 to 4 fins) were investigated. Their results show that the Nusselt number is increased by 6 to 9 times for 30° inclined angle. Tian and Zhao [14] studied the heat transfer in PCMs embedded in porous metals. Due to the low thermal conductivity of PCMs, one way to improve their thermal conductivity is using a metal porous medium. Coupled equations including conduction and natural convection are considered. The results show that using a porous medium increases conductivity but weakening the buoyancy effects. Zhao et al. [15] studied heat transfer in encapsulated PCM for thermal energy storage. The PCM was NaNO_3 and encapsulated by stainless steel. They showed that the heat transfer rate is impacted by

the size of the capsule, the type of the working fluid, and the buoyancy-driven effects in the molten PCM, which can reduce the storage time. Ebrahimi [16] investigated the effect of the mixture of CuO nanoparticles and a PCM, on the performance of the photovoltaic module, experimentally. This study shows that using pure PCM reduces the surface temperature of the photovoltaic cells from 58.34°C to 51.7°C . Convective heat transfer of slurry PCM in a Tube with butterfly tube inserts has been studied by Moshtagh et al. [17]. They showed, adding microencapsulated PCM to pure water in a pipe under constant heat flux improves the heat transfer rate up to 41%. Azadi et al. [18] studied solar wall equipped with photovoltaic cells and PCMs numerically. They reported that the best thickness for the PCM layer on the wall is 0.05m and the optimum airflow rate is 0.04 kg/s. Also, increasing the PCM thickness reduces energy efficiency.

As mentioned in the above works [1-18], PCMs are being used to cover the existing lag between the supplied and demanded energy. They have a large heat capacity and increase thermal inertia. Then using them will reduce the energy consumption in the different parts of the industry. In this paper, heat transfer and fluid flow in a channel equipped by two pipes containing PCM has been studied numerically. The results consist of two parts. In the first part, the PCM is in phase change mode (melting). In this part, the best diameter and location of the pipe (containing PCM) will be found. In the second part, the temperature of the PCM will change with time. The results of the second part are obtained for the optimum size and position which have obtained in the first part and are include the time required for the temperature of the PCM to reach 99% of the temperature of the working fluid. This final time is important. Because after it, heat transfer from the fluid to the PCM stops, and the PCM must be charged beforehand.

2- Governing Equations and Boundary Conditions

The geometry of the channel and two pipes containing PCM which are perpendicular to the flow direction is depicted in Fig. 1. In this study, the flow is laminar, steady-state, incompressible, and two-dimensional. The Reynolds numbers are 500 and 700 and the Prandtl numbers of the working fluids are assumed to be 0.7, 1.4, 3. The results of this study can be used for cooling the mini or microchannels with high temperatures. Avoiding high-pressure drop, and, due to the small dimensions in this channels Reynolds number is in the laminar region and due to high temperature the Prandtl number is between 0.7 for air and 3 for hot water.

Due to symmetry, the half part of the channel has been solved. For grid generation and solution in body fitted mesh, there are different strategies. One of them is using C-type mesh [19] as shown in Fig. 2 and the second one is using two-parts mesh as shown in Fig. 3. The C-type mesh has some weaknesses such as unnecessary compressing grids near the inlet, outlet boundaries, and symmetric line. Also, the results of the inlet boundary which has more effects on the solution domain will not influence the solution domain in a good manner. Avoiding these weaknesses, the two-parts solution domain has been selected (Fig. 3). In this strategy, the solution

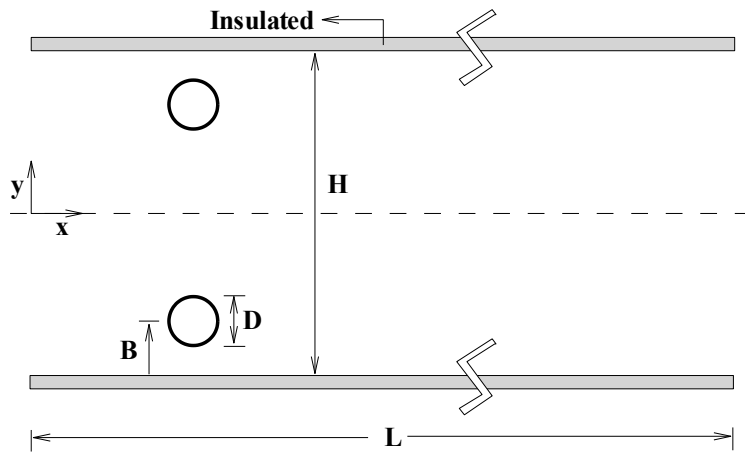


Fig. 1. The geometry of the channel and the pipes containing PCM

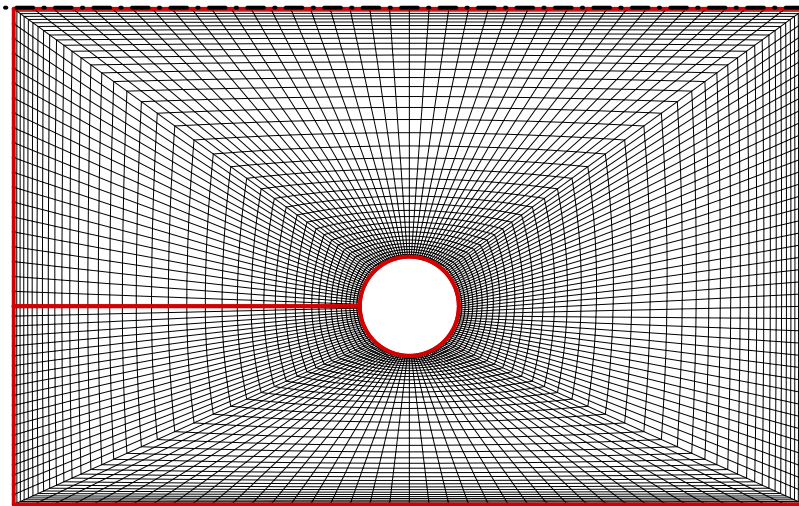


Fig. 2. C-type generated mesh

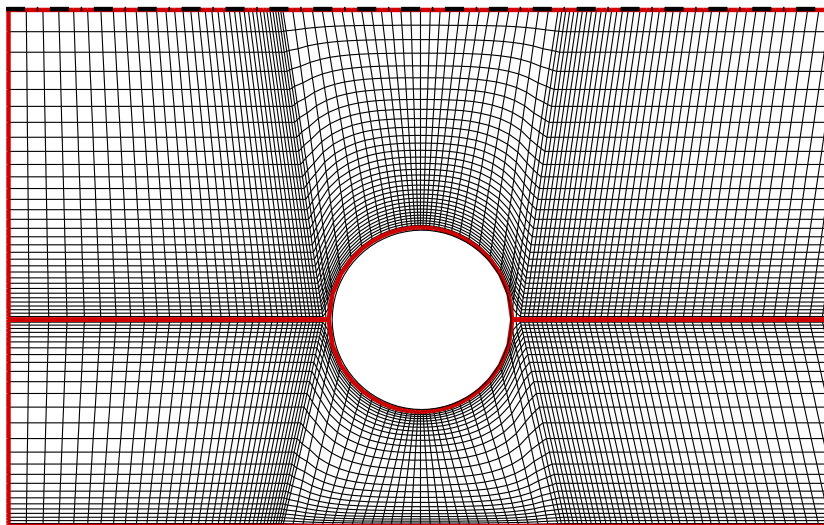


Fig. 3. Two parts generated mesh

of the interface for each part is applied as a boundary condition for another part. On the other hand, these parts have an overlap in their interface.

Because of the non-Cartesian generated grid (Fig. 3), the governing equations including continuity, Navier-Stokes, and energy, are transformed from the physical domain to the computational domain by the chain derivation as obtained by [19, 20]. By introducing the following non-dimensional parameters:

$$\begin{aligned} x_i &= \frac{X_i}{H}, d = \frac{D}{H}, b = \frac{B}{H}, \\ t^* &= \frac{U_b t}{H}, u_i = \frac{U_i}{U_b}, p = \frac{P}{\rho_f U_b^2} \\ T &= \frac{\theta - \theta_{0-PCM}}{\theta_{in} - \theta_{0-PCM}}, Re = \frac{\rho_f U_b D}{\mu}, \\ Pr &= \frac{\mu c_p}{k}, Pe = Re \cdot Pr \end{aligned} \tag{1}$$

The general form of Navier-Stokes and energy can be expressed as follows [19, 20]:

$$\begin{aligned} \frac{\partial \psi}{\partial t^*} + \frac{\partial u^c \psi}{\partial \xi} + \frac{\partial v^c \psi}{\partial \eta} = \\ JS_\psi + \left[\frac{\partial}{\partial \xi} \left(\frac{Jq_{11}}{Pe} \psi_\xi \right) + \frac{\partial}{\partial \eta} \left(\frac{Jq_{22}}{Pe} \psi_\eta \right) \right] + \\ \left[\frac{\partial}{\partial \xi} \left(\frac{Jq_{12}}{Pe} \psi_\eta \right) + \frac{\partial}{\partial \eta} \left(\frac{Jq_{12}}{Pe} \psi_\xi \right) \right] \end{aligned} \tag{2}$$

where ψ is dependent variables such as “u”, “v”, and “T”. Then, the flow is regarded steady while heat transfer is considered unsteady. The first term in the left side is the temporal term for energy equation and due to the independency of momentum equations on temperature, it is zero for Navier-Stokes equations. The other terms of the left side are convective terms. The first term of the right side (JS_ψ) is a source term such as pressure gradient and other terms of the right side are the diffusion terms. The explanations of parameters, which have been used in this equation are explained in [19, 20].

The temperature of the PCM in the pipe is considered to be lumped. It will happen when the PCM container (pipes) are equipped by the pins [8] or filled by a porous medium [14] with high thermal conductivity. These pins or mediums increase the conductivity of the PCM and prevent the recirculation due to the buoyancy effect and allow us to suppose lumped temperature for the PCM. After phase change duration (melting mode) the temperature of the pipe is increased

by the following relation from energy conservation,

$$(mc_p)_{PCM} \frac{d\theta_{PCM}}{dt} = \dot{Q} \tag{3}$$

where \dot{Q} is the heat transfer rate from working fluid to the pipe and is equal to,

$$\dot{Q} = (\dot{m}c_p)_f (\theta_{b-in} - \theta_{b-out}) = (\dot{m}c_p)_f \Delta\theta_b \tag{4}$$

which $\Delta\theta_b$ if the bulk temperature change of the fluid flow. Combining Eqs. 3 and 4 and using dimensionless parameters and doing some simplifications, leads to,

$$\frac{dT_{PCM}}{dt^*} = \frac{(\rho c_p)_f}{(\rho c_p)_{PCM}} \frac{4}{\pi d^2} \Delta T_b \tag{5}$$

It is supposed that the thermal conductivity of the wall of the pipe is high. Then it doesn't need to solve the conduction heat transfer in the body of the pipes as a conjugate problem.

2- 1- Boundary conditions

On the channel and the pipe walls, the no-slip condition is applied, and to find out the effect of the PCM presence, the channel walls have been supposed to be insulated. Due to the symmetry, in the middle of the channel, the following relation has been applied:

$$\left. \frac{\partial \psi}{\partial y} \right|_{y=0} = 0, \tag{6}$$

Where ψ denotes the velocity components, pressure, and temperature.

It is supposed that the velocity profile is fully developed before arriving at the inlet boundary and will be fully developed again at the outlet boundary. Then, the boundary conditions at inlet and outlet boundaries, are expressed as follows,

$$\begin{aligned} u(0, y) = 1.5y(1-y), v(0, y) = 0, T(0, y) = 1, \\ \left. \frac{\partial u}{\partial x} \right|_{x=L^*} = 0, v(L^*, y) = 0, \left. \frac{\partial T}{\partial x} \right|_{x=L^*} = 0 \end{aligned} \tag{7}$$

where L^* is the channel length and in each case, it is chosen so that the flow is fully developed at the end of the channel.

Table 1. Grid independency

	f	$Pe\Delta T_b$	Max. error%
294×42	0.0540	76.3931	10.3
312×52	0.0531	70.3842	1.6
328×62	0.0530	69.2631	-

Table 2. Code validity

	e/D	f/D	g/D	ϕ°	Nu_s
Ref. [26]	0.730	0.6	1.55	126.3	-
Ref. [27]	-	-	-	-	6.25
Present study	0.725	0.6	1.55	126.0	6.38
error%	0.7	0	0	0.2	2

3- Numerical Method

The finite volume method on a collocated grid is used to solve the governing equations. Avoiding central cell pressure independency, the interpolation of the Rhie and Chow [21] has been applied. For the temporal terms in the energy equations, the fully implicit scheme [22] and for convective terms, the hybrid differencing [23] are used. Finally, the Semi-Implicit Method for Pressure Linked Equations (SIMPLE) [24] applied to solve the discretized algebraic equations using line by line method. To solve the equations, three computer codes in FORTRAN have been written. The first one is a grid generation code, the second one solves the flow field by SIMPLE method. The results of the flow field are used to solve the energy equation in the third code. To sense the higher gradients, the generated grid is more compressed near the walls.

Results in the next section are based on the friction coefficient (f) and change in the fluid bulk temperature using the following formulas,

$$T_b = 2 \int_{y=0}^{y=0.5} uTdy \tag{8}$$

The heat transfer rate from the working fluid to the PCM can be calculated by Eq. (4). Also, in this equation $\dot{m} = \rho U_b H \times 1$ is the mass flow rate and is equal to $Re \cdot \mu$. then,

$$\dot{Q} = (Re \cdot \mu) c_p (\theta_{in} - \theta_{block}) \Delta T_b \tag{9}$$

and, $\mu c_p = kPr$, then

$$\dot{Q} = Pr k (\theta_{in} - \theta_{block}) Re \cdot \Delta T_b = k (\theta_{in} - \theta_{block}) Pe \cdot \Delta T_b \tag{10}$$

Finally,

$$\frac{\dot{Q}}{k(\theta_{in} - \theta_{block})} = Pe \cdot \Delta T_b \tag{11}$$

Then, the $Pe \cdot \Delta T_b$ determines the heat transfer rate from the fluid to the PCM.

In the convective heat transfer, engineers avoid the pressure drop coefficient (f) but try to increase the heat transfer rate. Then based on the Reynolds analogy [25] it is better to compare the heat transfer rate to the Pressure Drops Ratio (HPR) for different parameters to find out the optimum state, based on Eq. (12).

$$HPR = \frac{Pe \cdot \Delta T_b}{f} \tag{12}$$

The grid independency of results including the friction factor (f) and heat transfer rate is carried out by running the codes for different point numbers at $Re=700$, $Pr=3$, $b=0.175$, $d=0.165$. The results are reported in Table 1. It is clear that the grid with 312×52 points with a maximum error of less than 2% is suitable to run the codes.

To verify the results, the flow field and heat transfer around an isothermal cylinder in a free stream for airflow at $Re_D=40$ has been solved. The non-dimensional geometrical parameters and the Nusselt number in the stagnation point have been compared with the other studies [26, 27] in Table 2. The Nusselt number in [27] has been obtained by the following equation,

$$Nu_s = 1.14 Pr^{0.4} Re_D^{0.5} \tag{13}$$

where ϕ is the separation angle.

4- Results and Discussions

Streamlines for a fixed diameter ($d=0.178$) in different situations at $Re=700$ have been shown in Fig. 5. For small values b , the tube acts as a barrier near the wall, and a large vortex forms behind it. By increasing the distance from the wall, two recirculation zones will have configured. More increase in the pipe distance from the wall causes bigger recirculation in the domain. These significant differences in the streamlines' shape will lead to different behavior in the heat transfer.

The temperature contours for different parameters have been shown in Fig. 6. It is clear that the Reynolds and Prandtl numbers and the geometrical parameters including (b, d) have sensitive effects on the temperature contours.

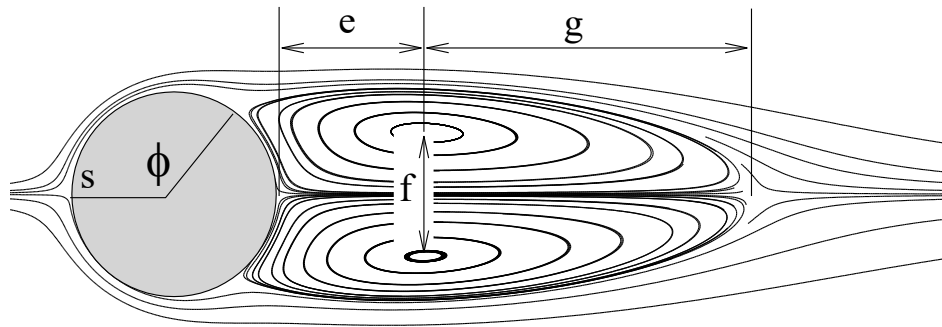
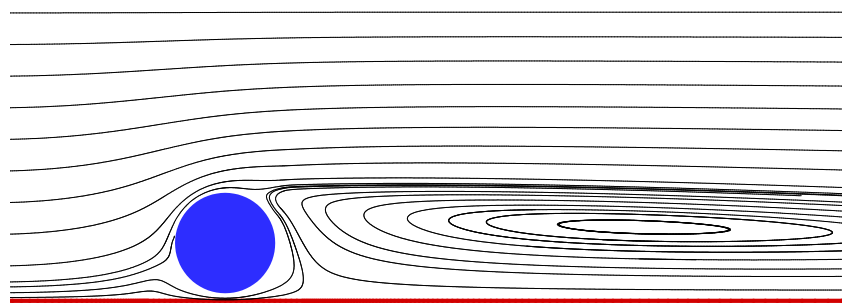
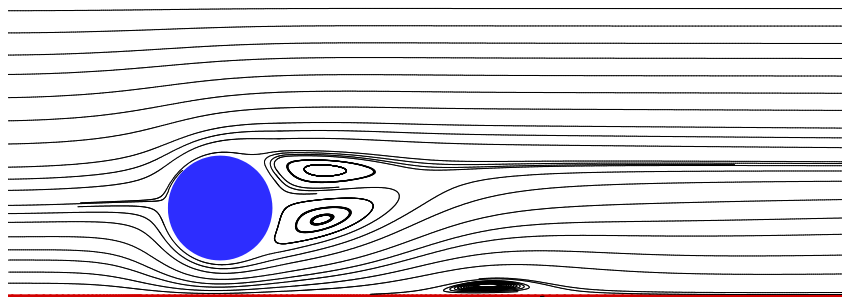


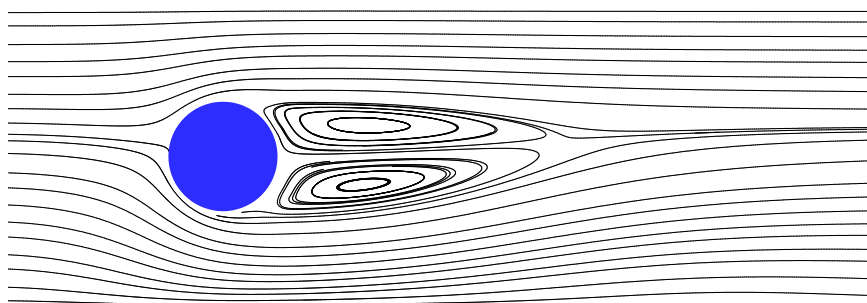
Fig. 4. The streamlines obtained in the present study for $ReD=40$, $Pr=0.7$



$b=0.1$

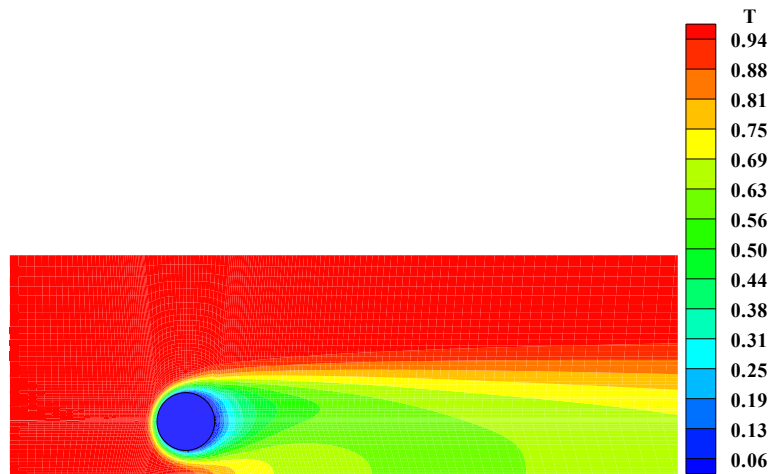


$b=0.125$

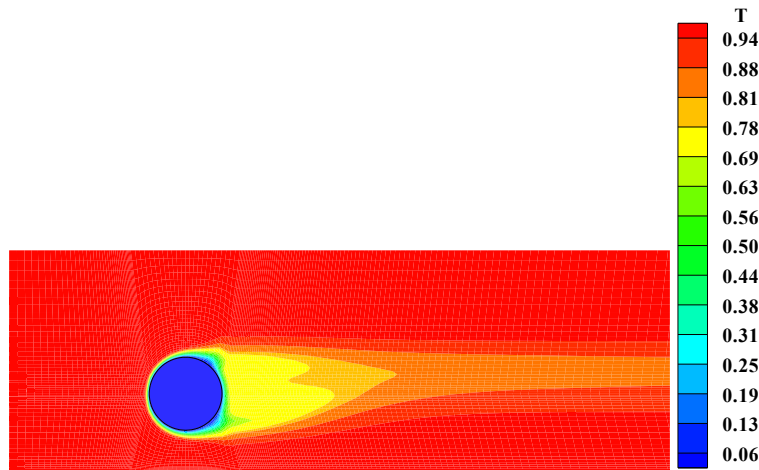


$b=0.25$

Fig. 5. Streamlines at $Re=700$ and $d=0.178$ for different pipe distances from the wall



$Re=500, Pr=0.7, b=0.125, d=0.127$



$Re=700, Pr=3.0, b=0.175, d=0.165$

Fig. 6. Temperature contours for different parameters

For a given Reynolds and Prandtl number, the friction factor and the heat transfer rate have been shown in Fig. 7 (a, b). But, as shown in Fig. 7(a, b), the rate of increase in the friction factor and the heat transfer are differing. It is due to the complicated behavior of the fluid flow and heat transfer as shown in Figs. 5 and 6.

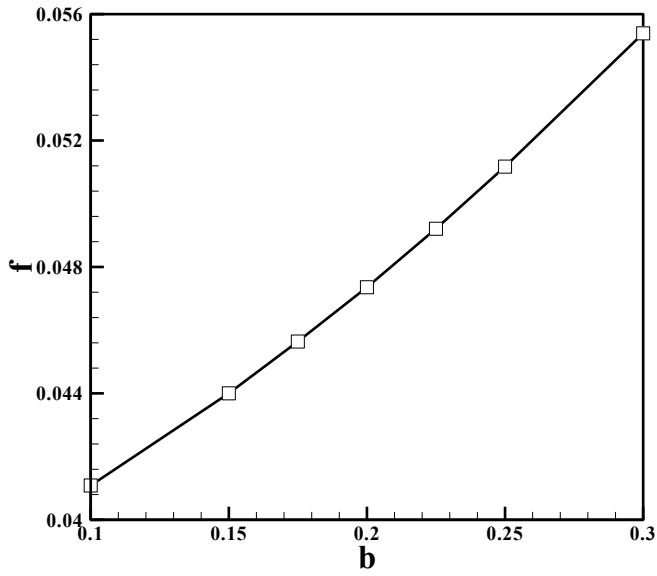
Due to the complicated behaviors and because of the presence of the recirculation zones and non-linear governing equations (Eq. (2)) including momentum and energy equations, the HPR has a maximum value for a certain distance from the wall ($b=0.15$) as shown in Fig. 7(c).

This behavior of HPR and its changing by diameter is depicted in Fig. 8. In this figure at a certain distance from the

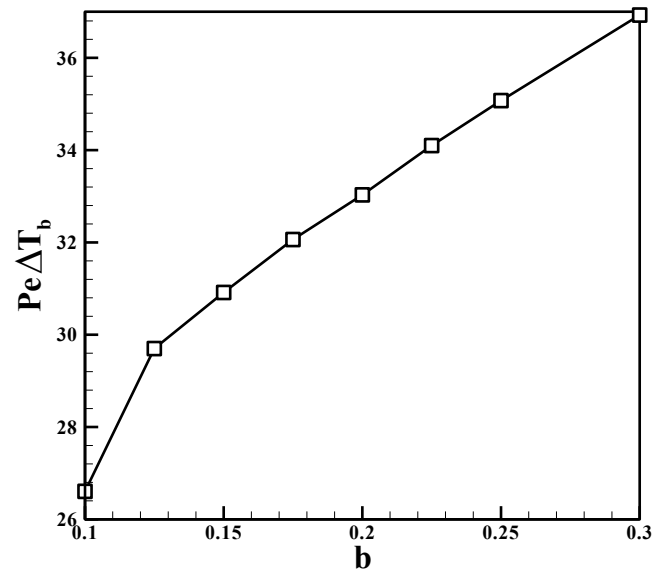
wall, the diameter varies from 0.127 to 0.178. It is clear that there is a maximum value for HPR at $d=0.153$. By increase in diameter, the friction factor increases nonlinearly but the heat transfer rate increases linearly. Then, such as “ b ”, also, there is an optimum value for diameter.

In Fig. 9, the effect of the Prandtl number on HPR in different Reynolds numbers has been illustrated. It is clear that the HPR increases by Prandtl number and there is an optimum state for each Prandtl number.

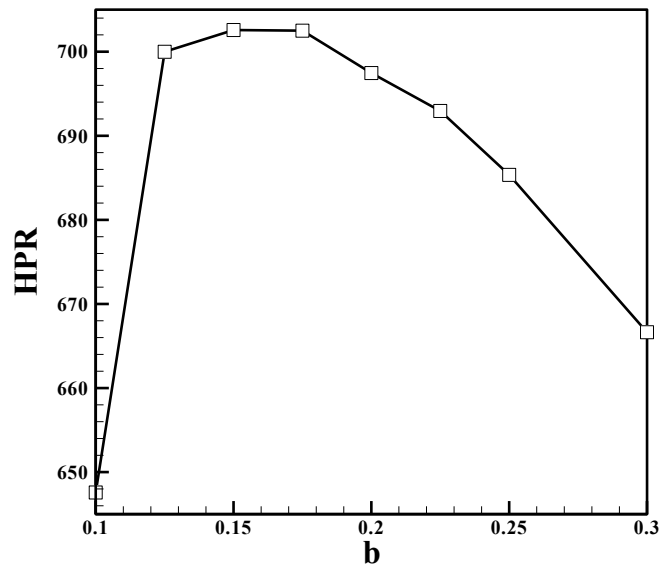
The computer code has been run for different Reynolds numbers (500,700), Prandtl numbers (0.7, 1.4, 3), diameters (0.153-0.178), and distances from the channel wall (0.1-0.3) and the optimum results (6 states) are tabulated in Table 3.



(a)

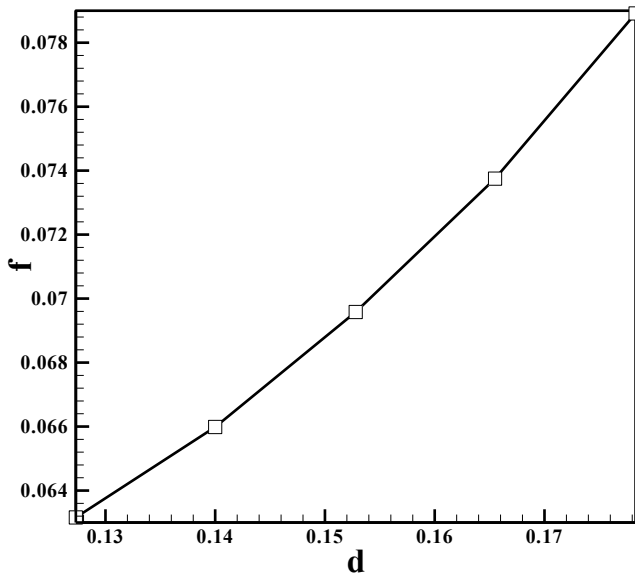


(b)

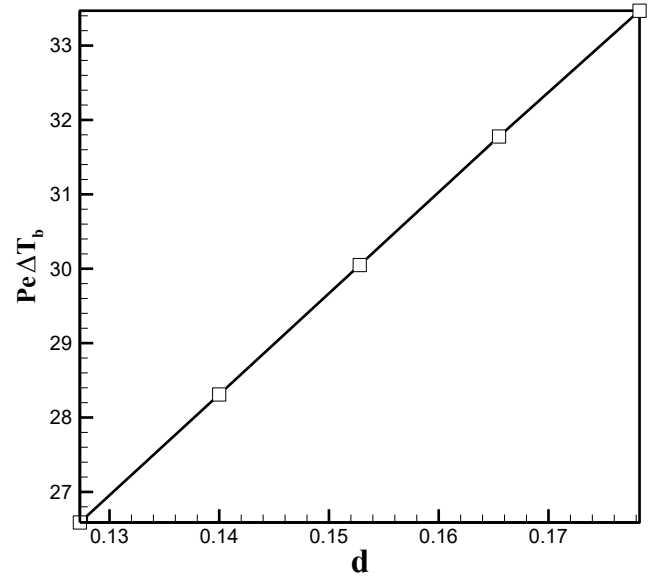


(c)

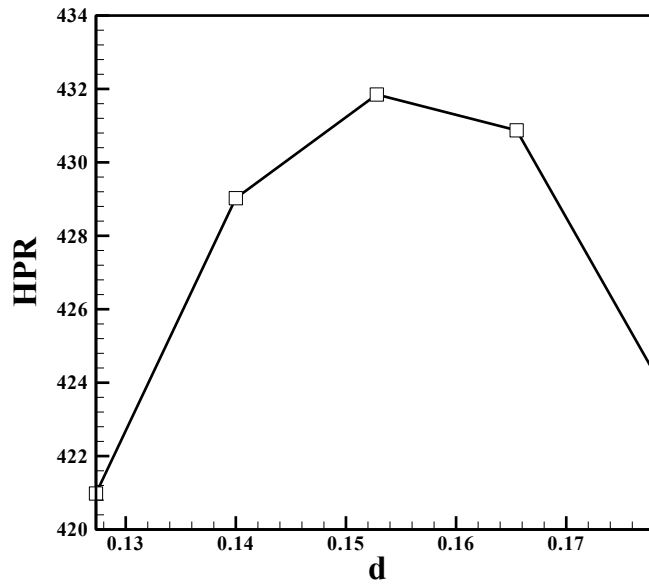
Fig. 7. (a) Friction factor (b) Change in bulk temperature (c) HPR for $Re=700$, $Pr=0.7$, $d=0.127$ vs. the pipe distance from the wall



(a)



(b)



(c)

Fig. 8. (a) Friction factor (b) Change in bulk temperature (c) HPR for Re=500, Pr=0.7, b=0.15 vs. pipe diameter

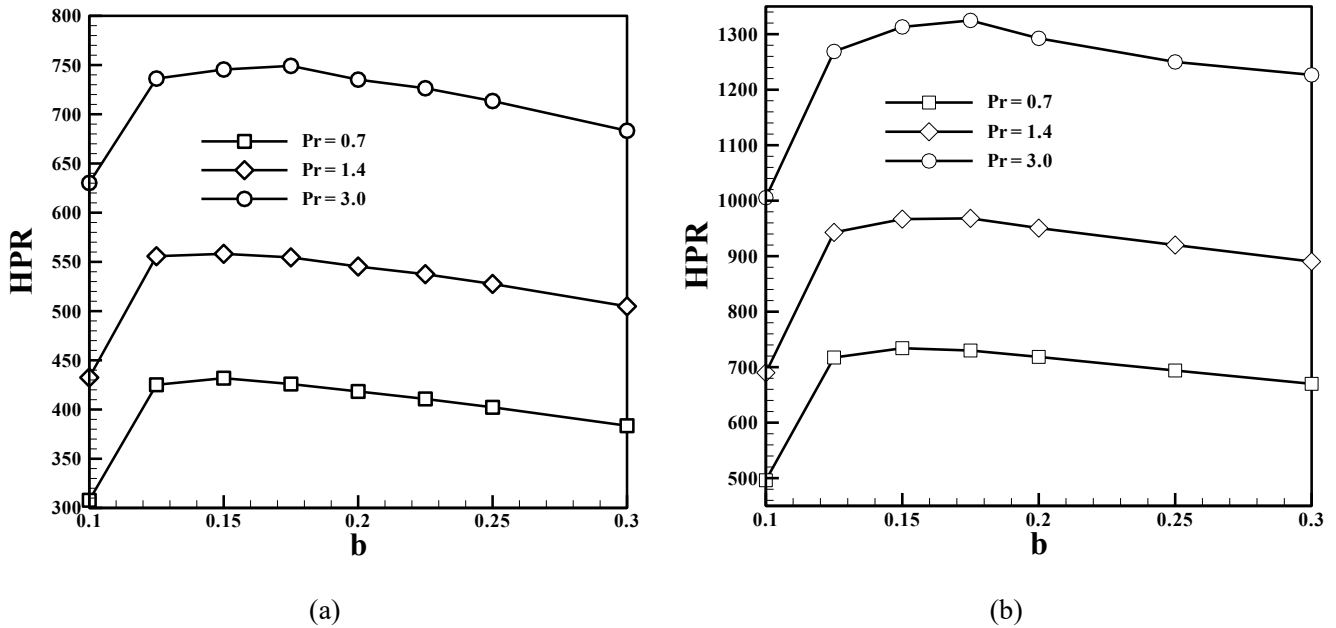


Fig. 9. HPR for (a) $Re=500, d=0.153$ (b) $Re=700, d=0.165$ at different Prandtl numbers

Table 3. The optimum states

		$Pr=0.7$	$Pr=1.4$	$Pr=3.0$
$Re=500$	b	0.15	0.15	0.175
	d	0.153	0.153	0.153
$Re=700$	b	0.15	0.175	0.175
	d	0.165	0.165	0.165

The second part of this section covers the unsteady states sensible heat transfer. The results of the second part are obtained for the optimum size and position which have been obtained in the first part as reported in Table 3. In this part, it is assumed that the PCM has been melted completely, and by getting more heat its temperature increases. Then as expressed in Eq. (5) the effect of the specific thermal capacity of the PCM to the working fluid or $(\rho c_p)_r$ is studied. Fig. 10, shows the time dependent temperature of the PCM and the fluid flow in $Pr=0.7, Re=700, b=0.15, d=0.153$ and $(\rho c_p)_r = 10^3$. It is obvious that the difference between the temperature of the PCM and fluid flow decreases and the shape of the temperature contours changes by time marching. The rate of this change is dependent on the different parameters.

The effects of the $(\rho c_p)_r$ on the temperature of the PCM

and the heat transfer from the fluid flow to the PCM is depicted in Figs. 11 to 16. The required time for the temperature of the PCM to reach 0.99 (t_s) increases by $(\rho c_p)_r$ and is defined in these figures. It means that by increasing in special thermal capacity ratio the temperature increasing rate decreases and the temperature of the PCM increases slowly. This behavior is also, visible in the fluid flow temperature increasing as a function of the special thermal capacity ratio. The rate of the temperature increasing at the first step times is high but by approaching the steady-state the temperature increasing step will decrease. The reason for this trend in temperature changing is related to the value of $(\rho c_p)_r$. It means that the high value of the PCM special heat capacity results in a low rate of temperature change. Because when the $(\rho c_p)_r$ is high, the heat received to the PCM does not have a lot of effect on the temperature.

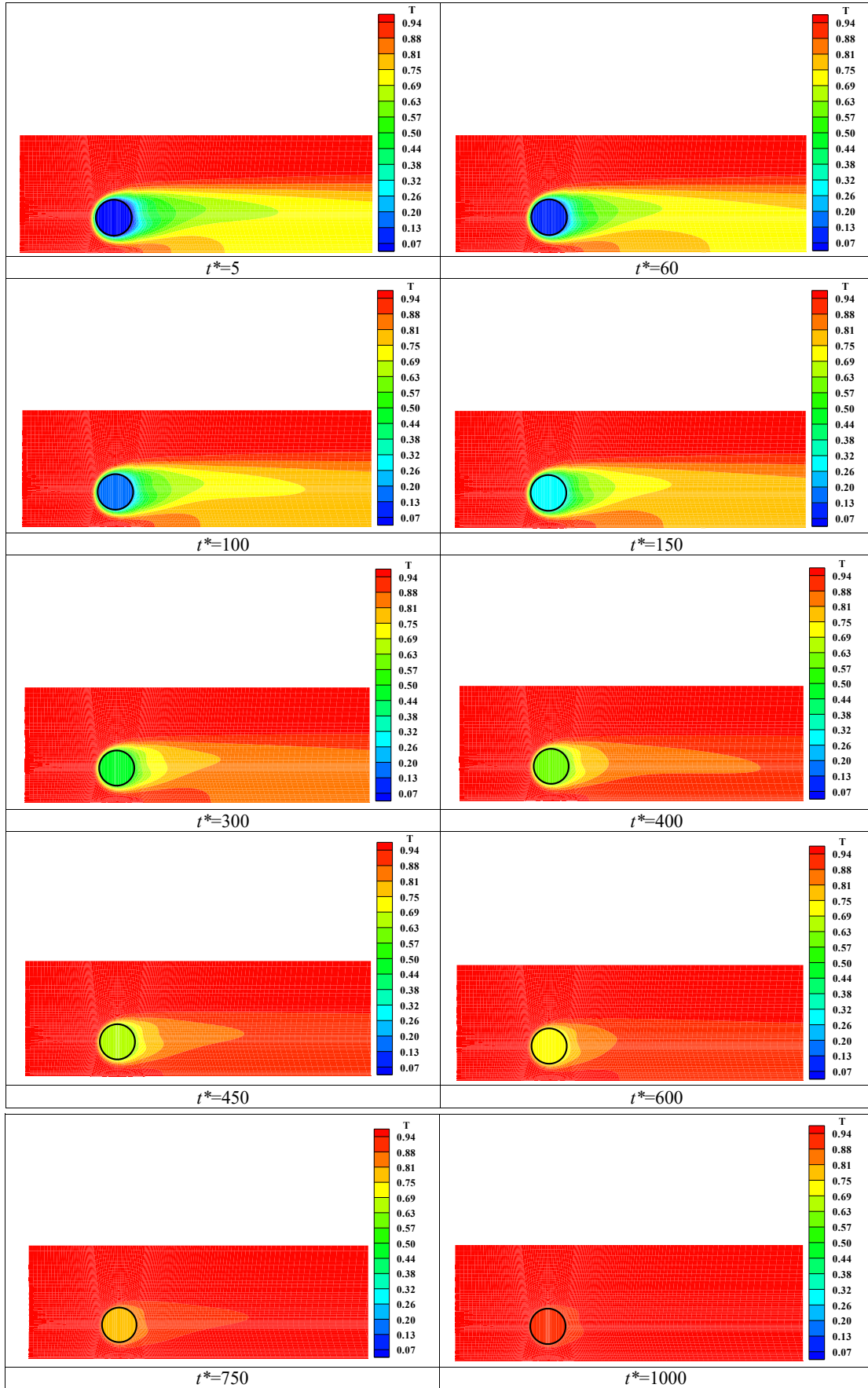


Fig. 10. Temperature contours for $Re=500$, $Pr=0.7$, $d=0.153$, $b=0.15$, $(\rho c_p)_r = 10^3$ at different times

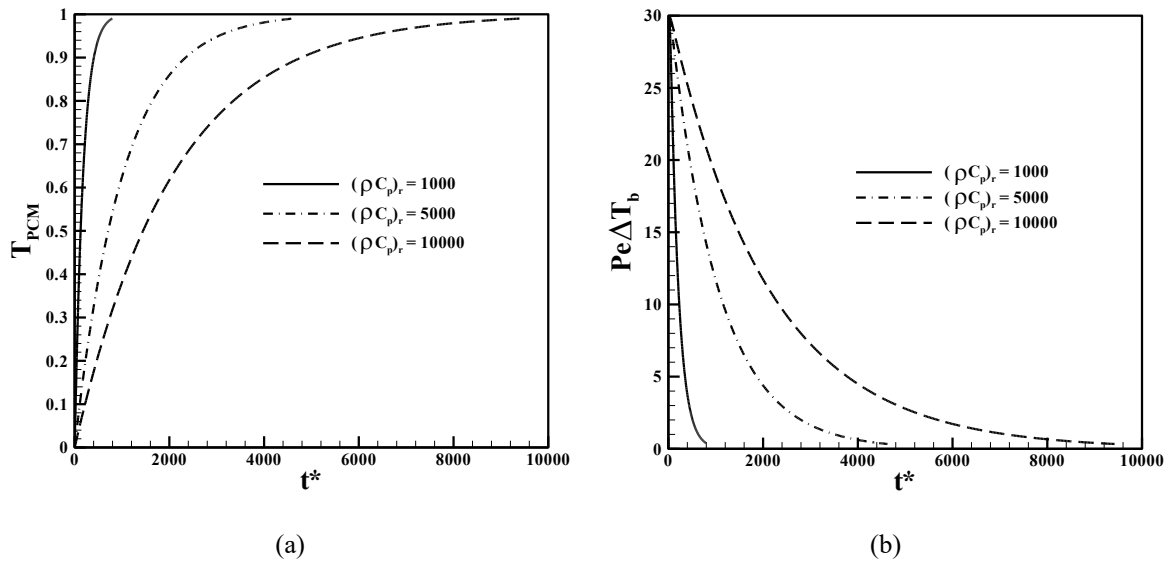


Fig. 11. The variations of (a) the PMC's and (b) the fluid bulk temperature at $Re=500$, $Pr=0.7$, $d=0.153$, $b=0.15$ at different $(\rho C_p)_r$ vs. time

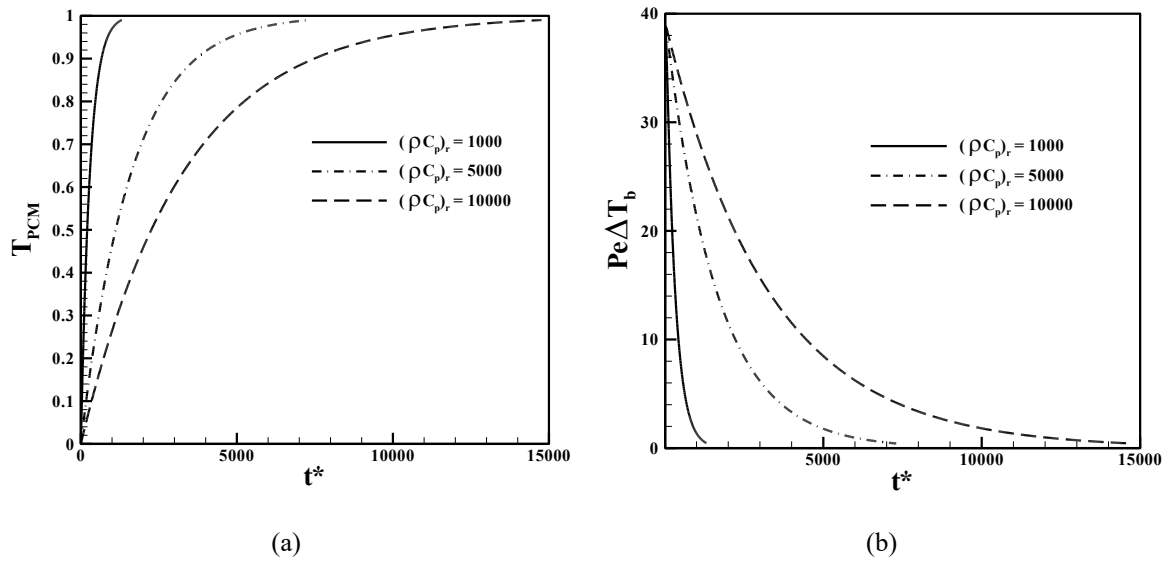


Fig. 12. The variations of (a) the PMC's and (b) the fluid bulk temperature at $Re=500$, $Pr=1.4$, $d=0.153$, $b=0.15$ at different $(\rho C_p)_r$ vs. time

Fig. 11, Shows the temperature variation of the PCM by time in different $(\rho C_p)_r$ and heat transfer rate to it, at $Re=500$, $Pr=0.7$, $d=0.153$, $b=0.15$ as an optimum state. As shown, “ t_s ” are 800, 4600, and 9600 for $(\rho C_p)_r = 1000, 5000, 10000$ respectively.

Fig. 12, Shows the temperature variation of the PCM by time in different $(\rho C_p)_r$ and heat transfer rate to it, at $Re=500$, $Pr=1.4$, $d=0.153$, $b=0.15$ as an optimum state. As shown, “ t_s ” are 1300, 7200, and 14900 for $(\rho C_p)_r = 1000, 5000, 10000$ respectively. In comparison with Fig. 11 which was for $Pr=0.7$,

it is clear that “ t_s ” increases by increasing in Prandtl number. But the heat transfer value (Figs. b) also increased. On the other hand, the heat transfer rate increases by increasing the Prandtl number. For $(\rho C_p)_r = 10000$ and $Pr=0.7$ the $Pe\Delta T_b$ decreases from 30 to zero in $t^*=9600$ but for $Pr=1.4$ it decreases from 38.2 to zero in $t^*=14900$. Then, for $Pr=0.7$ the ratio of $\frac{Pe\Delta T_b}{t_{max}^*}$ is about 0.003 but for $Pr=1.4$ this ratio is

about 0.025. It means that in the higher Prandtl number the heat transfer rate is more.

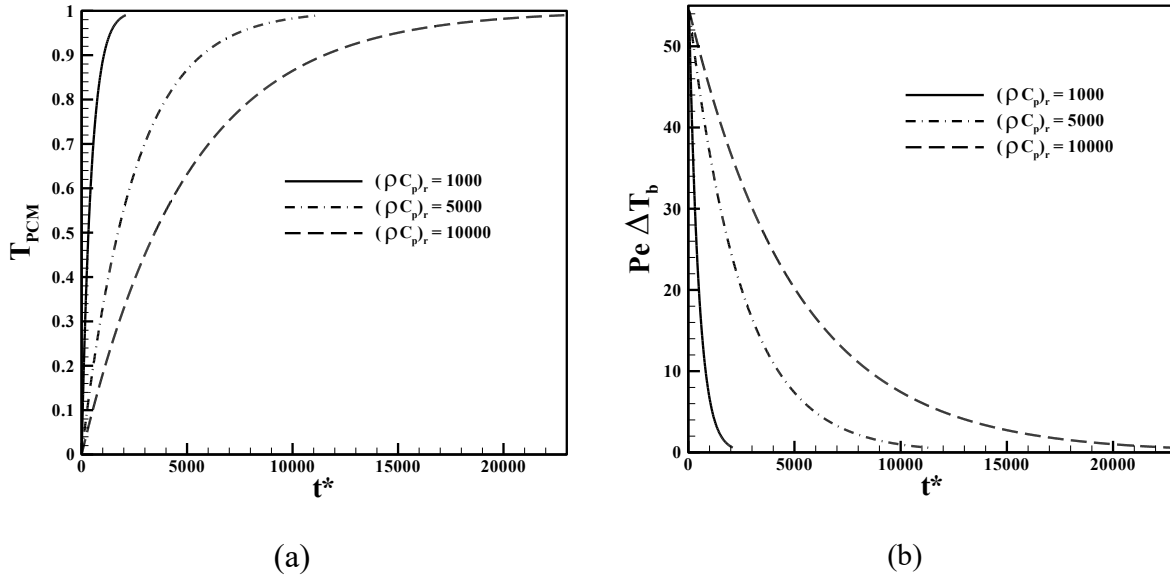


Fig. 13. The variations of (a) the PMC's and (b) the fluid bulk temperature at $Re=500$, $Pr=3$, $d=0.153$, $b=0.175$ at different $(\rho c_p)_r$ vs. time

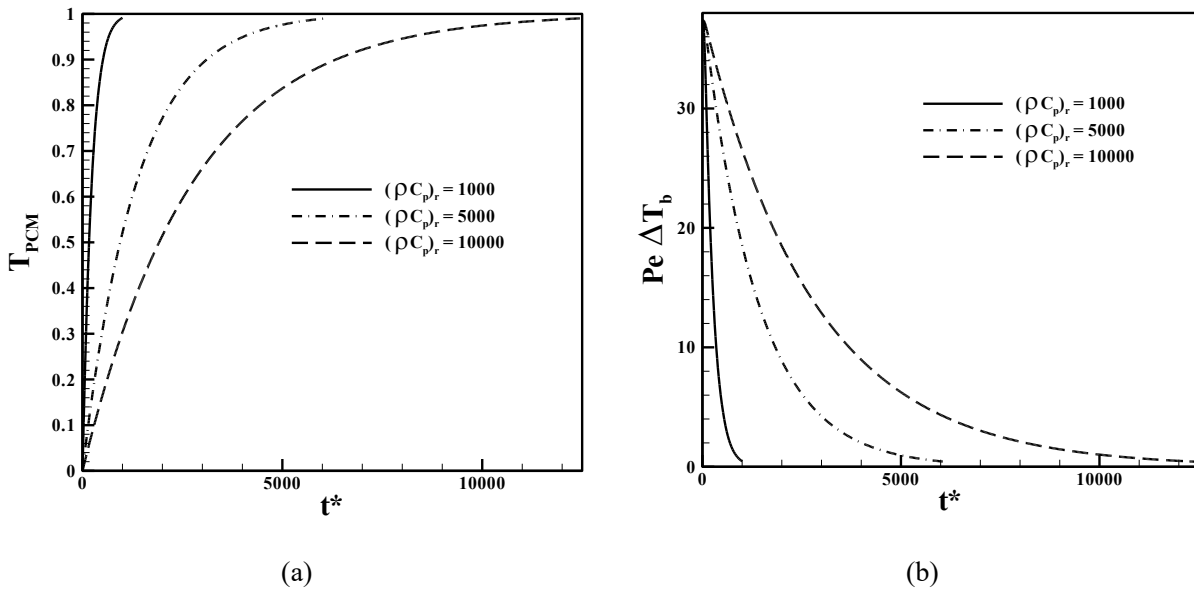


Fig. 14. The variations of (a) the PMC's and (b) the fluid bulk temperature at $Re=700$, $Pr=0.7$, $d=0.165$, $b=0.15$ at different $(\rho c_p)_r$ vs. time

Fig. 13, Shows the temperature variation of the PCM by time in different $(\rho c_p)_r$ and heat transfer rate to it, at $Re=500$, $Pr=3$, $d=0.153$, $b=0.175$ as an optimum state. As shown, " t_s " are 2050, 11500, and 23000 for $(\rho c_p)_r = 1000, 5000, 10000$ respectively. Due to the different Prandtl numbers and different distances of the pipe from the wall (b) these results cannot be compared with the results of Figs. 11 and 12. But, in this case, the ratio of $\frac{Pe \Delta T_b}{t_{max}^*}$ is about 0.0023 which presents a higher heat transfer rate.

Figs. 14 to 16 are a repetition of the results of Figs. 11 to 13, except that Figs. 14 to 16 are plotted for $Re = 700$. Fig.

14, shows the temperature variation of the PCM by time in different $(\rho c_p)_r$ and heat transfer rate to it, at $Re=700$, $Pr=0.7$, $d=0.165$, $b=0.15$ as an optimum state. As shown, " t_s " are 1000, 6100, and 12400 for $(\rho c_p)_r = 1000, 5000, 10000$ respectively.

Figs. 15 and 16, show the temperature variation of the PCM by time in different $(\rho c_p)_r$ and heat transfer rate to it, at $Re=700$, $d=0.165$, $b=0.175$ as an optimum state. Fig. 15 refers to $Pr=1.4$ and Fig. 16 refers to $Pr=3$. Also, in these cases, for $(\rho c_p)_r = 10000$ the ratio of $\frac{Pe \Delta T_b}{t_{max}^*}$ for $Pr=1.4$ is about

0.0027 and for $Pr=3$ is about 0.0024. which confirms that in the higher Prandtl number the heat transfer rate is higher.

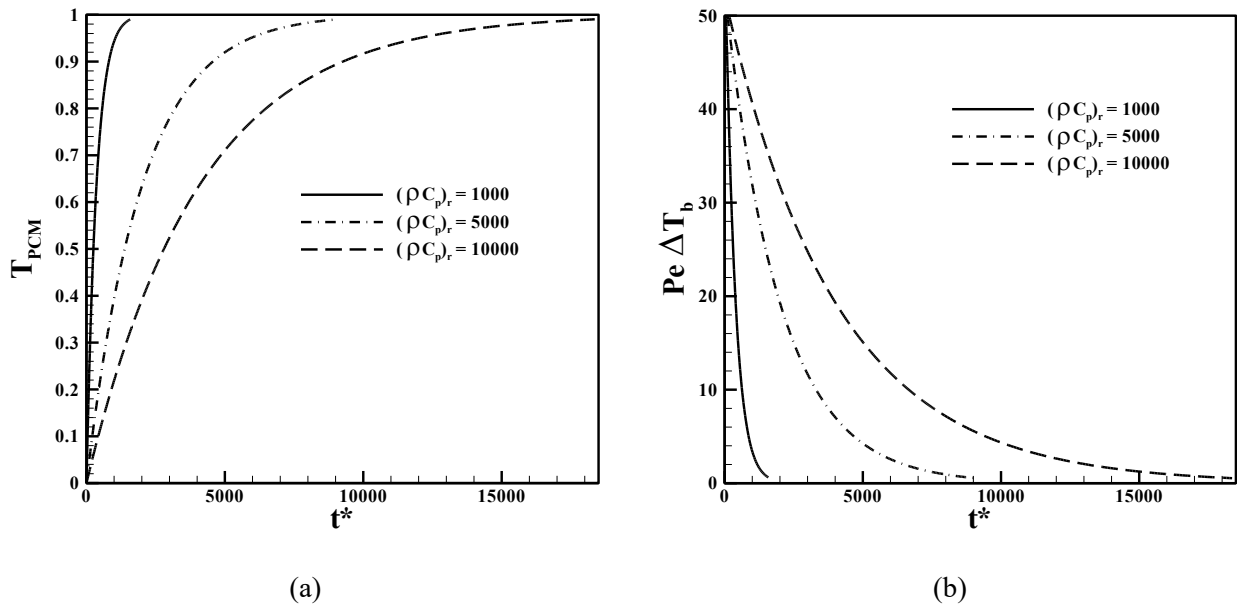


Fig. 15. The variations of (a) the PCM's and (b) the fluid bulk temperature at $Re=700$, $Pr=1.4$, $d=0.165$, $b=0.175$ at different $(\rho C_p)_r$ vs. time

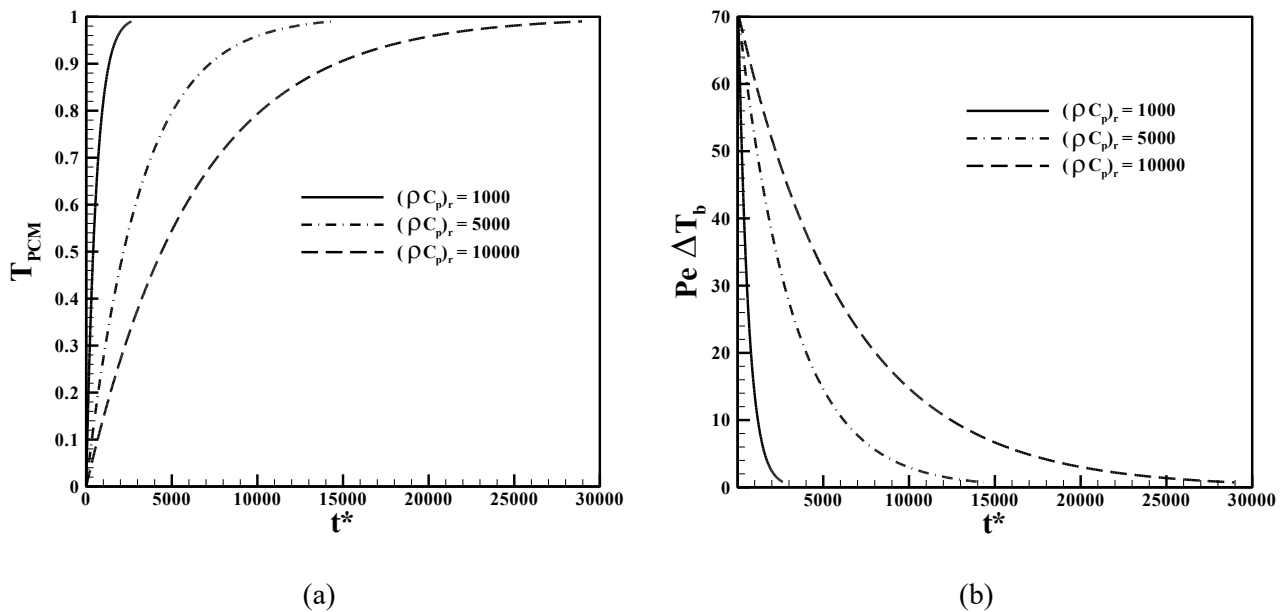
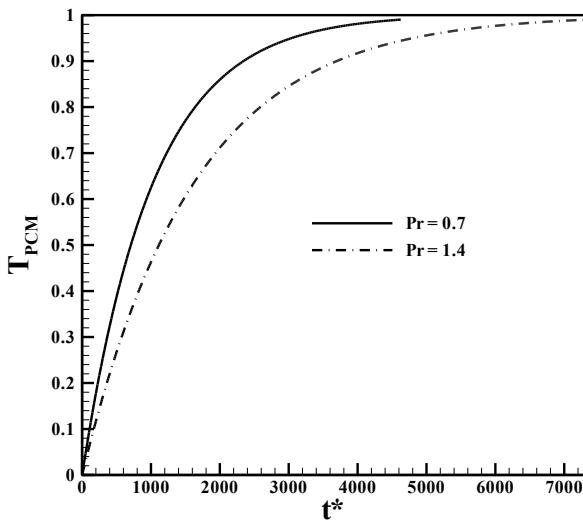


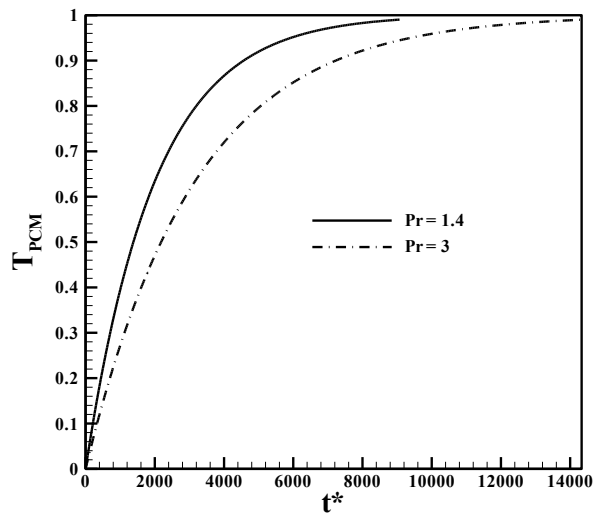
Fig. 16. The variations of (a) the PCM's and (b) the fluid bulk temperature at $Re=700$, $Pr=3$, $d=0.165$, $b=0.175$ at different $(\rho C_p)_r$ vs. time

The effect of the Prandtl number with the same geometrical parameter has been shown in Fig. 17. The larger the Prandtl number, the longer time it takes to reach a steady state. It means that the convective heat transfer coefficient is

higher in a higher Prandtl number. Then in a higher Prandtl number, the temperature increase step is low and it is favorable behavior for heat transfer purposes.



$Re=500, b=0.15, d=0.153$



$Re=700, b=0.175, d=0.165$

Fig. 17: Effect of Prandtl number on the final time for $(\rho c_p)_r = 5000$

5- Conclusions

In this paper, a channel equipped by two pipes filled with PCMs has been studied numerically. The governing equation including continuity, momentum, and energy in fluid flow have been solved by the control volume method (SIMPLE) in curvilinear coordinate. In the first part, the PCM is in the phase change state (melting) and the optimum states (diameter and the distance of the pipes from the channel walls) in different Reynolds and Prandtl numbers obtained. The best non-dimensional diameters of pipes are 0.153 for $Re=500$ and 0.165 for $Re=700$ in different Prandtl numbers. Also, the best non-dimensional distance of pipes from wall is between 0.15 and 0.175 for different Reynolds and Prandtl numbers. In the second part (after the melting process) which refers to the sensible heat transfer, the temperature of the PCM increases by time and is supposed to be lumped. Then the energy equation in the fluid flow is unsteady. The results of this part are have been obtained for the optimum states obtained in the first part and report the required time for PCM to reach the temperature of the fluid flow. This time is depending on the Reynolds number, Prandtl number, and the special thermal capacity of PCM to the fluid flow ratio or $(\rho c_p)_r$. By increase in this ratio the required time increases. It means that if the special heat capacity of the PCM will be high, the fluid temperature will rise lower which is a favorable behavior in heat transfer applications. Also, an increase in Reynolds and Prandtl numbers increases the heat transfer rate and it results in a low temperature raising rate.

Nomenclature

b, B	the distance of the pipe from the channel wall, m
c_p	heat capacity, $J.kg^{-1}.K^{-1}$
d, D	Diameter, m
f	friction factor
H	height of the channel, m
HPR	Heat transfer rate to Pressure drop Ratio
J	Jacobian of the coordinate transformation
k	thermal conductivity, $W.m^{-1}.K^{-1}$
L	non-dimensional channel length
m	Mass, kg
\dot{m}	flow mass rate, $kg.s^{-1}$
p, P	non-dimensional and dimensional pressure, Pa
Nu	Nusselt number
Pe	Peclet number
Pr	Prandtl number
\dot{Q}	heat transfer rate, W
Re	Reynolds number based on H
Re_D	Reynolds number based on D
t	time, s
t_s	nondimensional required time for the temperature of the PCM to reach 0.99

T	non-dimensional temperature
U, V	velocity component in x, y directions, $m.s^{-1}$
u, v	non-dimensional velocity component in x, y directions
X, Y	x, y coordinate, m
x, y	non-dimensional x, y coordinate

Greek Symbols

ξ, η	curvilinear coordinate components
θ	temperature, K
μ	viscosity, Pa.sec
ρ	density, $kg.m^{-3}$
ϕ	separation angle, $^{\circ}$
ψ	general variable (u, v, p, T)
$\Delta\theta_b$	the bulk temperature change of the fluid flow

Superscripts

C	contravariant velocities
*	non-dimensional time and length

Subscripts

B	fluid bulk value
F	fluid
In	inlet
out	outlet
PCM	phase change material
S	stagnation point
0	value at the initial time

References

- [1] Y. Hu, P. K. Heiselberg, H. Johra and R. Guo, Experimental and Numerical Study of a PCM Solar Air Heat Exchanger and its Ventilation Preheating Effectiveness, *Renewable Energy*, 145 (2020) 106-115.
- [2] R. J. Khan, M. D. Z. H. Bhuiyan, D. H. Ahmed, Investigation of Heat Transfer of a Building wall in the Presence of Phase Change Material (PCM), *Energy and Building Environment*, 1 (2020) 199-206.
- [3] M. Arici, F. Bilgin, S. Nizetic, H. Karabay, PCM integrated to external building walls: An optimization study on maximum activation of latent heat, *Applied Thermal Engineering*, 165 (2020) 114560.
- [4] A. N. Desai, A. Gunjal and V. K. Singh, Numerical investigations of fin efficacy for phase change material (PCM) based thermal control module, *International Journal of Heat and Mass Transfer*, 147 (2020) 118855.
- [5] G. Chen, G. Sun, D. Jiang, Y. Su, Experimental and numerical investigation of the latent heat thermal storage unit with PCM packing at the inner side of a tube, *International Journal of Heat and Mass Transfer*, 152 (2020), 119480.
- [6] A. R. Mazhar, A. Shukla, S. Liu, Numerical analysis of rectangular fins in a PCM for low-grade heat harnessing, *International Journal of Thermal Sciences* 152 (2020) 106306.
- [7] M. Aadmi, M. Karkri, M. E. Hammouti, heat transfer characteristics of thermal energy storage for PCM (phase change material) melting in horizontal tube: Numerical and experimental investigations, *Energy*, 85 (2015) 339-352.
- [8] S. Aziz, N. A. M. Amin, M. S. Abdul Majid, M. Belusko, F. Bruno, CFD simulation of a TES tank comprising a PCM encapsulated in sphere with heat transfer enhancement, *Applied Thermal Engineering*, 143 (2018) 1085-1092.
- [9] L. F. Cabeza, H. Mehling, S. Hiebler, F. Ziegler, Heat transfer enhancement in water when used as PCM in thermal energy storage, *Applied Thermal Engineering*, 22 (2002) 1141-1151.
- [10] C. R. Chen, A. Sharma, S. K. Tyagi, D. Buddhi, Numerical heat transfer studies of PCMs used in a box-type solar cooker, *Renewable Energy*, 33 (2008) 1121-1129.
- [11] T. T. Chow, Y. Lyu, Numerical analysis on the advantage of using PCM heat exchanger in liquid flow window, *Applied Thermal Engineering* 125 (2017), 1218-1227.
- [12] Z. Khan, Z. A. Khan, P. Sewell, Heat transfer evaluation of metal oxides based nano-PCMs for latent heat storage system application, *International Journal of Heat and Mass Transfer*, 144 (2019), 118619.
- [13] T. Sathe, A. S. Dhoble, Thermal analysis of an inclined heat sink with finned PCM container for solar applications, *International Journal of Heat and Mass Transfer*, 144 (2019), 118679.
- [14] Y. Tian, C. Y. Zhao, A numerical investigation of heat transfer in phase change materials (PCMs) embedded in porous metals, *Energy*, 36 (2011), 5539-5546.
- [15] W. Zhao, A. F. Elmozughi, A. Oztekin, S. Neti, Heat transfer analysis of encapsulated phase change material for thermal energy storage, *International Journal of Heat and Mass Transfer*, 63 (2013), 323-335.
- [16] E. Ebrahimi, Experimental Investigation of Cooling Performance Enhancement of a Photovoltaic Module Using a Phase Change Material-CuO Nanoparticles, *Amirkabir Journal of Mechanical Engineering*, 52 (2) (2018) 281-296.
- [17] M. Moshtagh, A. Jamekhorshid, A. Azari, H. Bazaee, An Experimental Investigation of Convective Heat Transfer of Slurry Phase Change Material in a Tube with Butterfly Tube Inserts, *Amirkabir Journal of Mechanical Engineering*, 52 (6) (2020) 1561-1576.
- [18] N. Azadi, F. Sarhaddi, F. Sobhnamayan, Thermal Analysis of a Solar Wall Equipped with Photovoltaic Cells and Phase-Change Materials, *Amirkabir Journal of Mechanical Engineering*, DOI: 10.22060/mej.2019.16268.6315.
- [19] K. A. Hoffman, *Computational Fluid Dynamics for Engineers*, Engineering Education System, Austin, Texas (1989)
- [20] M. Raisee, *Computation of Flow and Heat Transfer*

- Through Two- and Three-Dimensional Rib-Roughed Passages, (1999), Ph.D. Thesis, Department of Mechanical Engineering, University of Manchester (UMIST)
- [21] C. M. Rhie, W.L. Chow, Numerical Study of the Turbulent Flow Past an Airfoil with Trading Edge Separation, *AIAA J.*, 21 (11) (1983) 1525-1535.
- [22] H. K. Versteeg, W. Malalasekera, *An Introduction to Computational Fluid Dynamics: The Finite Volume Method*, Harlow, England: Pearson Education Ltd, (2007)
- [23] D. B. Spalding, A Novel Finite Difference Formulation for Differential Expressions Involving Both First and Second Derivatives, *International Journal of Numerical Mathematics Engineering*, 4 (1972) 551-559.
- [24] S. V. Patankar and D.B. Spalding, A Calculation Procedure for Heat, Mass and Momentum Transfer in Three-Dimensional Parabolic Flows, *International Journal of Heat and Mass Transfer*, 15 (1972), 1787-1806.
- [25] J. P. Holman, in: *Heat Transfer*, eighth ed. McGraw-Hill Inc., New York (1997), pp. 218-282.
- [26] K. Taira, T. Colonius, The immersed boundary method: A projection approach, *Journal of Computational Physics*, 225 (2007) 2118–2137.
- [27] A. Bejan, *Convection Heat Transfer*, John Wiley& Sons, Hoboken, New Jersey, 4th ed. (2013)

HOW TO CITE THIS ARTICLE

J. Rostami, Optimum Diameter and Location of Pipes Containing Phase Change Materials in a Channel in Latent and Sensible Heat Transfer, AUT J. Mech Eng., 5 (4) (2021) 599-616.

DOI: [10.22060/ajme.2021.18362.5896](https://doi.org/10.22060/ajme.2021.18362.5896)



